Trends in the Centroid of the Northern Hemisphere's Circumpolar Vortex

Nazla Bushra and Robert V. Rohli

Department of Oceanography & Coastal Sciences, College of the Coast & Environment,
Louisiana State University, Baton Rouge, LA 70803-4105
Corresponding Author: Nazla Bushra (nbushr1@lsu.edu, 0000-0002-7007-0456)

Key Points:

- Daily distance that the Northern Hemispheric circumpolar vortex centroid moves decreases linearly over time, with distinctive seasonality.
- The centroid tends to be displaced toward the Pacific basin, likely due to the influence of warm Atlantic Ocean circulations.
- These results are important because they suggest that they index the mid-tropospheric response to observed surface warming.

Abstract

Recent previous research has established the "sharpest gradient" approach to defining the circumpolar vortex and has identified correlations of the area and circularity of the Northern Hemisphere's circumpolar vortex (NHCPV) to important atmospheric-oceanic teleconnections. However, because geographical shifts in the NHCPV, independent of area or circularity changes, could affect surface environmental conditions, this research addresses the question of the extent to which the NHCPV centroid undergoes such shifts, both intra- and inter-annually. Results show that during the 1979–2017 period, the centroid has moved less on a daily basis in more recent years, perhaps indicative of a stabilization in circulation, with semi-annual and seasonal periodicities in the daily distance moved. A consistent preference toward the Eastern Hemisphere is evident by the displacement of the centroids toward the Pacific basin throughout the study period. Collectively, these results indicate the mid-tropospheric response to the near-surface warming.

Plain Language Summary

Our previous research developed an approach for delineating the leading edge of the boundary of the cold polar air circulation. This research identifies the position of the center of this polar circulation in the Northern Hemisphere, on a daily basis, from 1979 through 2017. We find that this centroid's position has stabilized over time while maintaining a preferred position on the Eastern Hemisphere side of the North Pole. These results are important because they suggest that the middle-to-upper weather layer in the atmosphere may responding slowly to the near-surface warming over the last few decades.

Keywords

Circumpolar Vortex; centroid; daily distance; emerging hot spot analysis; seasonal cycle; trend analysis

1 Introduction

1.1 The circumpolar vortex

The two tropospheric circumpolar vortices (CPVs, Waugh et al., 2017) – one approximately centered on each pole – represent the hemispheric-scale, steering, extratropical circulation at a given time. These strong, quasi-west-to-east (*i.e.*, quasi-westerly) extratropical wind belts circumnavigate the north and south high-latitude regions at altitudes of 5−12 km. The leading edge of each CPV is near the steepest gradient of air temperature at the three-dimensional boundary where polar and tropical air meet. At any given time, 3−6 long waves (aka: Rossby waves, or planetary waves) exist in the westerly flow at the leading edge of the CPV in each hemisphere, at the core of the polar front jet stream (PFJ), that amplify/deamplify and propagate in response to thermal and orographic forcing, and subtropical upper-level divergence (Hoskins & Karoly, 1981).

This broad-scale steering atmospheric circulation represented by the CPVs is an important topic in geoenvironmental sciences because of its many links to environmental features at the surface, such as air mass properties (*e.g.*, Vanos & Cakmak, 2014), surface air temperature (*e.g.*, Moron et al., 2018) and wind (*e.g.*, van den Broeke & van Lipzig, 2002), sea surface temperature (SST; *e.g.*, Frauenfeld et al., 2005), water vapor transport (*e.g.*, Wang & Ding, 2009), precipitation (*e.g.*, Srinivas et al., 2018), ocean salinity (*e.g.*, Chen et al., 2018), storm tracks (*e.g.*, Kidston et al., 2015), sea-ice extent (*e.g.*, Orme et al., 2017), ozone (*e.g.*, Glovin et al., 2016), and other pollutants (*e.g.*, Bartlett et al., 2018).

Previous research (Bushra & Rohli, 2019) established the "sharpest gradient" approach to defining the CPV and correlated the area and circularity of the Northern Hemisphere's CPV (NHCPV) to important atmospheric-oceanic teleconnections. Using this definition, a library of daily NHCPV area and circularity has been constructed, based on 500-hPa geopotential heights, facilitating comparisons to previous research. While the recent surface warming may be linked to a temporally shrinking NHCPV, Martin (2015) found that for winter seasons of cold years, the 850-hPa NHCPV-driven jet was expanded equatorward in both the Pacific and Atlantic sectors of the Northern Hemisphere.

The shape of the NHCPV may have also changed under the recent warming, as it becomes more or less intertwined with areas of known air-sea interactions in the form of teleconnections (Bushra & Rohli, 2019). Recent research (Bushra & Rohli, 2019) has found that the NHCPV has become wavier over time and is positively correlated most closely with the indices of the Arctic Oscillation (AO; Thompson & Wallace, 1998) and North Atlantic Oscillation (NAO; Lamb & Peppler, 1987), and negatively with Pacific/North American (PNA; Wallace & Gutzler, 1981) teleconnection pattern.

The possibility of the NHCPV changing its orientation independently of areal or shape (i.e., circularity) changes invites further analysis. A simultaneous amplification or dampening of the ridge-trough configuration on both sides of the Northern Hemisphere simultaneously could create a large change in area and circularity while leaving the centroid in a static location. Likewise, the mean daily longitudinal progression or retrogression of the ridges and troughs could occur in the absence of changes in area or circularity; in such a case, only the centroid of the polygon representing the NHCPV would change. Thus, trends in NHCPV centroid locations may yield additional information about changes in ridge-trough location, either independently of, or in association with, areal and circularity changes.

To date, no research at the daily scale has addressed whether the NHCPV's centroid location has drifted or shifted over time. At the monthly scale, Rohli et al. (2005) and Wrona and Rohli (2007) showed that temporal variability and long-term change in the monthly mean NHCPV centroid location (and also area and circularity) are linked to Northern Hemisphere temperature variability and regional-scale flow patterns. But questions remain about how accurately and precisely the daily NHCPV can be represented and how the NHCPV variability impacts and is impacted by surface environmental features. This question is important because even in the absence of changes in area and/or circularity of the NHCPV, shifts in its daily position could easily cause redistribution of the energy associated with severe weather, which occurs on the daily scale, and/or a host of other high-frequency atmospheric/oceanic impacts.

1.2 Centroids in geospatial analysis

In geospatial analysis, centroid may imply either the geometric center or the center of mass of an areal feature. Various methods of determining a centroid (Deakin et al., 2002), including the spatial mean, the center of mass (or center of gravity), and the center of minimum distance, may yield substantially different results. All three measures are well-explained in Levine (2002) and De Smith et al. (2007). Deakin et al. (2002) also listed several methods for defining the centroid of a polygon on the geoid; for example, "moment centroid" refers the measure of the center of mass, "average centroid" relies on the arithmetic mean, root mean square, harmonic mean, geometric mean, median, and mode centroids, and others include the minimum bounding rectangle centroid, the negative buffer centroid, and the circle centroid.

While in climate science, a number of studies use the concept of "centroid" in cluster analysis (Steinbach et al., 2003, Cassou et al., 2004, Esteban et al., 2005, Zhang et al., 2009), others have used centroids to characterize a natural climatic region. For example, Haskett et al. (2000) produced daily, simulated weather datasets from general circulation models, for the nine climate centroids in Iowa. Liu et al. (2012) used centroids to represent daily mean evapotranspiration zones. And Frierson & Hwang (2012) and Donohoe et al. (2013) used centroids to specify centers of precipitation. Wrona and Rohli (2007) identified the NHCPV centroid using center of mass but only at the monthly scale.

2 Purpose

This research uses an objective method for identifying the centroid of the NHCPV defined in Bushra and Rohli (2019) via geospatial techniques. The centroid position is then examined for both temporal (at both high and low frequencies) and spatial (distribution and frequencies over places) changes. Results will identify both the impact of day-to-day hemispheric-scale fluctuations and long-term changes in the steering circulation that have accompanied the changes in surface temperature over the last several decades.

3 Data and Methods

As described more fully in Bushra and Rohli (2019), gridded 500-hPa geopotential heights from the National Centers for Environmental Prediction/U.S. Dept. of Energy Reanalysis Atmospheric Model Intercomparison Project (AMIP) II (NCEP-R2; Kanamitsu et al. 2002) data set are selected here, with analysis from 1979─2017. The study period is also segmented to 1979─2001, to correspond with that used in Wrona and Rohli's (2007) monthly analysis, and 2002─2017 subperiods. Then, the "center of mass" criterion (Deakin et al., 2002; De Smith et al., 2007) is used to identify the geographic coordinates of the centroid of each day's NHCPV, because of its wide acceptance and to correspond to the method used in Wrona and Rohli (2007). The North Polar Stereographic Projection (GISGeography, 2020) is used to preserve CPV shape.

3.1 Rationale of using the *center of mass*

Deakin et al. (2002) noted that in a vector- (point-) based system, although the "average centroids" formulas is the easiest legitimate way of measuring the spatial central tendency, the insensitivity to the order of the vertices, and thus the shape of the polygons, can be limiting for some types of analysis. The "minimum bounding rectangle centroid" approach (Deakin et al. 2002) can be unduly influenced by the four extreme vertices of the polygon, is subject to bias by outliers in general (De Smith et al. 2007),and is insensitive to the shape. Deakin et al. (2002) also concluded that (i) the "negative buffer" and circle centroid approaches fall short in handling irregular shapes, such as a CPV with amplified Rossby waves, and are difficult to compute, (ii) the "minimum distance centroids" approach has computational drawbacks and requires sophisticated function minimization software for calculation, and (iii) neither the "momentum" nor the "center of mass" approaches have such disadvantages, and they provide a more logical and intuitive measurement of the centroid for irregular polygon shapes.

In the "center of mass" approach, the centroid is a point defined in a manner analogous to the "balance point" of the distribution of mass of a corresponding body. According to this definition, and regarding the body as a plane area A of uniformly distributed material, the centroid position is

$$\overline{x}=\frac{M_y}{A} \quad \text{and} \quad \overline{y}=\frac{M_x}{A} \tag{1}$$

where M_x and M_y are (first) moments with respect to the x- and y-axes respectively (Ayres 1968).

3.2 Trend analysis

Trend analysis is performed to reveal the changes in centroid location over time seasonally, intra-annually, and inter-annually. For each day in the time series, the great circle distance that the centroid moved since the previous day is computed, using a time series of vectors representing the magnitude and direction of centroid migration since the previous day.

Three techniques are widely used for measuring the great circle distance: (1) spherical law of cosines (Robusto, 1957), (2) Haversine (Sinnott, 1984), and (3) Vincenty inverse (Vincenty, 1975). The first two methods consider Earth as a sphere and the later treats Earth as an ellipsoid. Using a spherical model gives errors typically up to 0.3%. Thus, the Vincenty inverse formula is selected because it provides accuracy as close as 1 millimeter.

Linear regression analysis is then performed to identify temporal trends in the daily migration of the NHCPV's centroid, expressed as the great circle distance moved from the centroid location on the previous day, for both the entire time series and for the two subperiods. Noise in the data series is removed by applying Butterworth (1930) low-pass filtering at a cutoff point of 0.01 to remove the higher frequencies, before applying the spectral analysis. The Butterworth filter smooths the daily NHCPV centroid distance from the previous day. Then, the time-series signal is decomposed into frequency space by applying spectral analysis (Koopmans, 1995) to identify variability in the magnitude and the cyclical trend. The fast Fourier transform (FFT; Welch, 1967) is run to identify whether the seasonal signal is amplifying, deamplifying, or has multiple phases of amplification/deamplification for three time periods.

In addition to the time series analysis which reveals any temporal trends in the centroid location stability, circular statistical analysis is applied to reveal temporal trends in the directional dispersion of the centroid positions around a unit circle. To apply Rao's Spacing Test (Rao, 1972) of uniformity, Cartesian angular dispersion of the centroid positions from the previous day is calculated. The test assesses whether the angular positions of the centroids show any signs of directionality or are indicative of a random scatter. In Rao's Spacing test, the null hypothesis implies that data are of a uniform distribution, while the alternate hypothesis is that the data demonstrate directionality. Because the test statistic of 132.60 (α=0.05) falls below the critical value of 136.94, the angle of direction moved has no directional trend, suggesting that a follow-up emerging hot spot analysis (EHSA) is required.

3.3 Patterns of centroid over space and time

Two components of the "Space Time Pattern Mining" toolbox in ArcGIS Pro are used to identify statistical "hot" and "cold" spots (with "hot (cold) spot" defined as a place of frequent (infrequent) NHCPV centroid location) and temporal persistence and trends in NHCPV centroid location over the simultaneous space-time dimensions. First, the "Create Space Time Cube" (CSTC) tool is used to generate three-dimensional bins and calculate annual centroid frequencies in each hexagonal-shaped bin with opposite vertices spaced 102.9 km apart and 39 layers of z-axis representing time (i.e., years). This bin size is optimized from an algorithm based on the spatial distribution of the centroids. The hexagonal shape ensures more uniform distances between neighbors than a quadrilateral, thereby minimizing distortion, making it advantageous for high latitudes.

Then, this space-time set of bins, and their corresponding NHCPV annual frequencies, is input into the "EHSA" tool, which identifies trends across space (i.e., from one bin to another across the x- and y-axes, via the Getis-Ord Gi* (pronounced "G-i-star"; i.e., "hot spot analysis"; Getis & Ord, 1992) test and time (i.e., from one bin to another over the z-axis, via Mann-Kendall rank-correlation statistics (Hamed & Rao, 1998). Significant spatiotemporal trends (i.e., hot spots or cold spots) are further characterized as persistent, increasing, or decreasing, to give 16 cluster patterns categorized as "new," "consecutive," "intensifying," "persistent," "diminishing," "sporadic," "oscillating," and "historical," each for "hot" or "cold" spots, in addition to the "no pattern detected" category. The formal definitions of these patterns is provided, with their resulting frequencies, in Table 1. The Getis-Ord Gi* test provides z-scores with p-values for each bin, based on neighborhood distance and neighborhood time step parameter values. The statistically significant high and low z-scores measure the intensity of the centroid clustering in comparison to its neighboring centroids. The Mann-Kendall test assesses the temporal frequency trend for each bin by assigning a +1, −1, or 0 to that bin if the frequency of centroid location for a given year is larger, smaller, or equal to (respectively) that of the previous year in the same bin. For each bin, this value is summed for each of the 39 pairs of consecutive years, with the rank-correlation identifying significance of the temporal frequency trends in that bin.

4 Results and Discussion

4.1 Trend analysis

4.1.1 Linear trend

Linear regression reveals a significantly decreasing trend (p-value < 0.0001) for all three time periods considered. Thus, over the 1979−2017, 1979−2001, and 2002−2017 periods, the NHCPV centroid daily distance from the previous day decreased by 21.27, 20.17, and 8.402 m day^{-1}, respectively (Figures 1 and 2). The decreasing trend is significant for each of the cases (p-value < 0.001) and more robust earlier than later in the study period. This implies that the NHCPV centroid position has stabilized over time, even as Northern Hemispheric mean surface temperatures have warmed abruptly over the 2002–2017 subperiod. One possible explanation is that the largely uniformly "warm-phase" Atlantic Multidecadal Oscillation (AMO; Kerr, 2000), AO, and NAO in the second subperiod would likely support a more consistent (poleward) position of NHCPV displacement over the Atlantic and (potentially) a simultaneous consistent (equatorward) displacement over the Pacific sector. The decreasing trend in daily distance moved (i.e., increasing consistency in centroid position) would have been most noticeable in the latter half of the 1979─2001 period, leading to a stronger decrease in daily distance moved in the first sub-period, with more stabilization in the latter sub-interval.

4.1.2 Seasonal cycle

Spectral analysis of the daily time series of centroid distance from the previous day reveals distinct periodicity of the centroid location, with high-frequency variability modes for all three time intervals considered. All three periods show two periodic signals which appear well above the uncertainty level (Figures 3 and 4) in the FFT analysis. In the full time series (1979─2017) and 1979─2001 subperiod, the stronger of the two signals is quarterly (near 0.01 day^{-1}, or 4 yr^{-1}), perhaps reflective of the four-season environment, while the weaker is semi-

annual (near 0.005 day^{-1}, or 2 yr^{-1}), suggestive of the cold-warm seasonal flow (Figures 3 and 4a). The latter subperiod (2002–2017) shows stronger semi-annual than quarterly amplitudes (Figure 4b). This result may suggest that the more stabilized location of the CPV in the latter sub-interval was accompanied by rather abrupt summer-winter shifts, rather than four-season shifts, perhaps because by that time the warmer halves of the transition seasons had begun to resemble the summer pattern. The full time series shows stronger semi-annual and quarterly amplitudes than in either sub-interval, perhaps because outliers may have a relatively smaller effect in the longer temporal period of analysis.

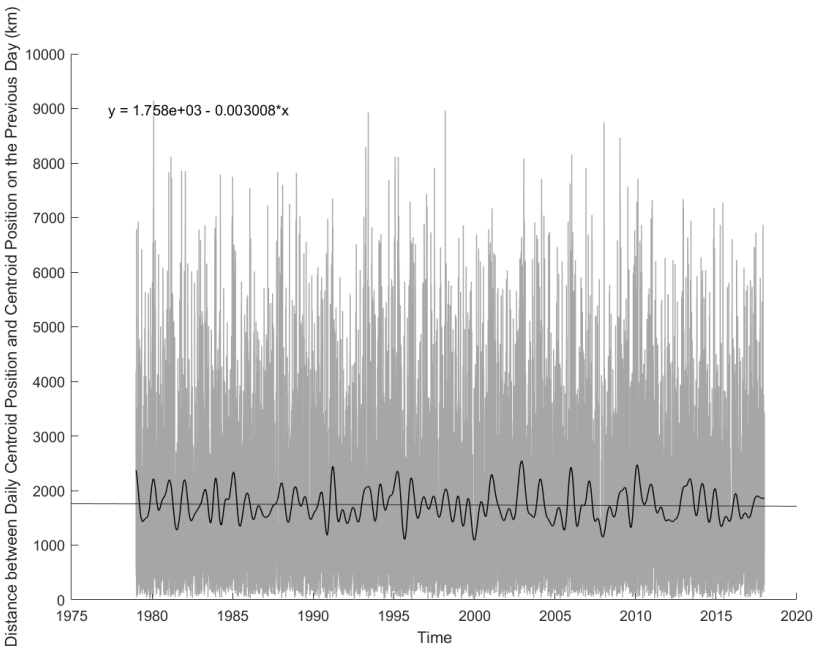

Figure 1. Time series of the daily NHCPV centroid distance migration from 1979 to 2017. The smoothed black line, from Butterworth low-pass filtering, shows the irregular annual cycle. The line depicts a statistically significant ($p<0.001$) decreasing trend.

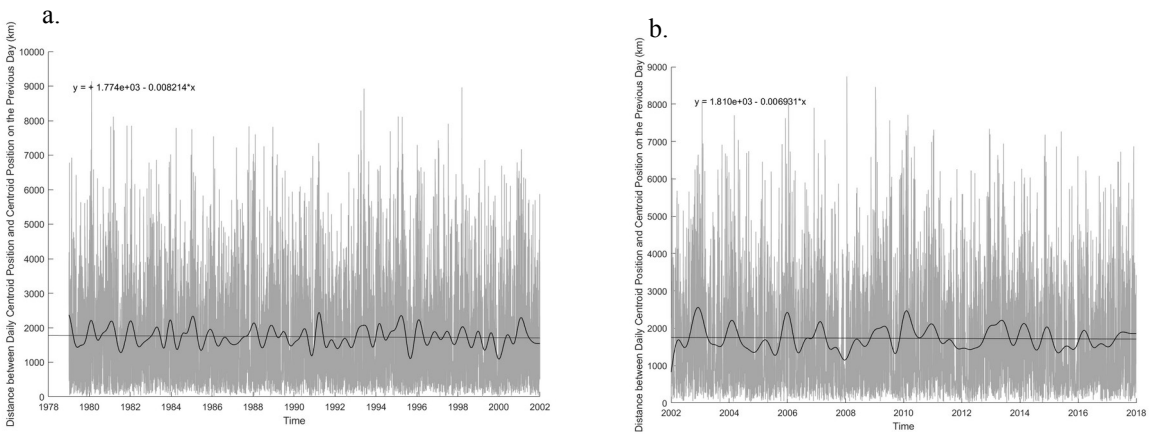

Figure 2. As in Figure 1, but for the (a) 1979–2001 and (b) 2002–2017 periods; the linear decreasing trends are statistically significant ($p<0.001$ in both cases).

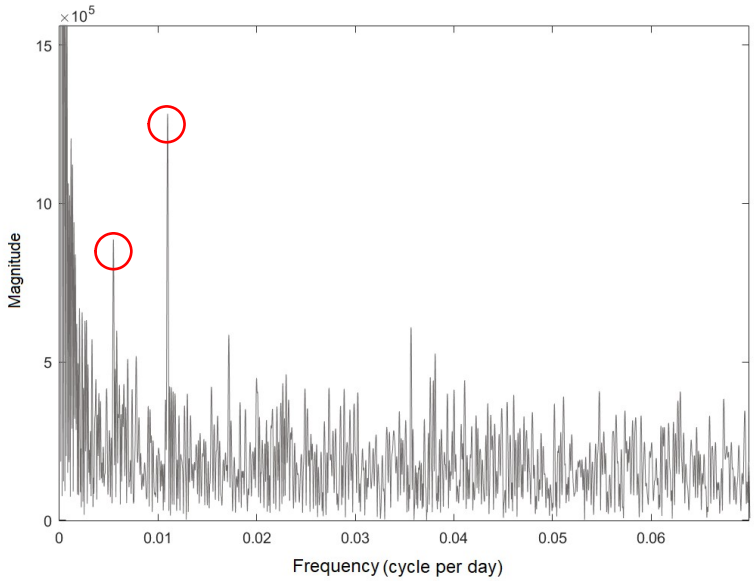

Figure 3. Magnitudes of the power spectra obtained by FFT analysis of the daily NHCPV centroid distance moved from the previous day (1979–2017). The red circles indicate the magnitude of the high-frequency variability. The left circle peaks at 0.00549 cycles per day, which is equivalent to 182.2 days. The right circle peaks at 0.01096 per day, which is equivalent to 91.2 days.

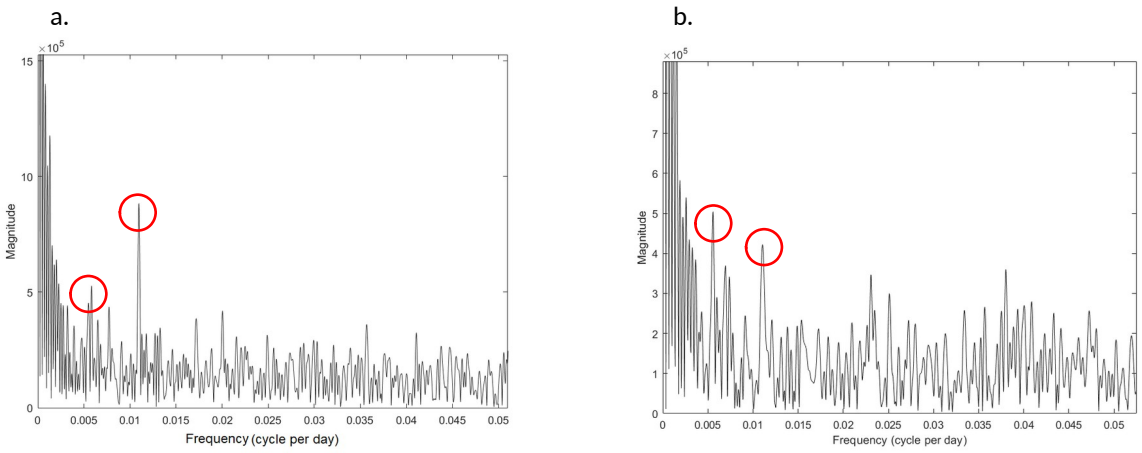

Figure 4. As in Figure 3, but for (a) 1979–2001, with peaks of 0.00582 and 0.01097 (at 171.7 and 91.2 days, respectively); and (b) 2002–2017, with peaks at 0.005538 and 0.01105 (180.6 and 90.5 days, respectively).

4.2 Centroid clustering patterns over space and time

The EHSA-derived frequencies of each hot/cold spot category, tabulated separately for the three time intervals, are shown in Table 1.

297 **Table 1.** Emerging hot spot (cold spot) pattern names and their definitions, and frequency of hot
298 spot bins, with cold spot bins in parentheses: (a) 1979─2017, (b) 1979─2001, and (c)
299 2002─2017 time periods. Source: Esri, 2020.
300

Pattern name	*Definition	(a) Number of bins (Total 3681)	(b) Number of bins (Total 1171)	(c) Number of bins (Total 1003)
No Pattern Detected	Does not fall into any of the hot or cold spot patterns (i.e., no significant trend)	2798	163	615
New Hot (Cold) Spot	Statistically significant (SS) hot (cold) spot for the final time step and has never been a SS hot (cold) spot before	5 (3)	0 (0)	10 (0)
Consecutive Hot (Cold) Spot	A single uninterrupted run of SS hot (cold) spot bins in the final time-step intervals. Location has never been a SS hot (cold) spot prior to the final hot (cold) spot run and < 90% of all bins are SS hot (cold) spots	3 (1)	0 (57)	0 (0)
Intensifying Hot (Cold) Spot	Has been a SS hot (cold) spot for ≥ 90% of the time-step intervals, including the final time step, while the intensity of clustering of high counts in each time step is increasing significantly	81 (0)	0 (0)	0 (0)
Persistent Hot (Cold) Spot	SS hot (cold) spot location for ≥ 90% of the time-step intervals with no discernible trend in the intensity of clustering over time	240 (0)	0 (0)	0 (0)
Diminishing Hot (Cold) Spot	SS hot (cold) spot location for ≥ 90% of the time-step intervals, including the final time step while the intensity of clustering in each time step is decreasing significantly	2 (0)	0 (0)	0 (0)
Sporadic Hot (Cold) Spot	An on-and-off-again hot (cold) spot location with < 90% of the time-step intervals having been SS hot (cold) spots and no time-step intervals being SS cold (hot) spots	201 (324)	0 (350)	1 (5)
Oscillating Hot (Cold) Spot	SS hot (cold) spot for the final time-step interval that has a history of also being a SS cold (hot) spot during a prior time step, with < 90% of the time-step intervals having been SS hot (cold) spots	14 (1)	0 (601)	368 (4)
Historical Hot (Cold) Spot	The most recent time period is not hot (cold), but ≥ 90% of the time-step intervals have been SS hot (cold) spots	8 (0)	0 (0)	0 (0)

301

302 Over the 1979─2017 period, centroid hot and cold spots are distributed widely, ranging
303 from north of the Bering Sea to south of Greenland; Figure 5 shows these along with their
304 EHSA-derived categories. Of the 3681 bins, 554, or 15.05 percent (329, or 8.94 percent) show a

statistically significant linear trend in their hot (cold) spot category (Table 1), for a total of 883 bins having a trend; the remaining 2798 bins (76.01 percent) show no pattern.

A trend for spatiotemporally increasing displacement of hot spots toward the Pacific basin over time is evident (Figure 5), supporting the notion of the influence of the AMO and NAO, especially in the second subperiod. Persistent (27.18 percent of the 883 bins with a trend) and Intensifying (9.17 percent) hot spots are over the Arctic Ocean basin, but mostly skewed toward the Pacific (Figure 5). A cluster of Oscillating hot spots (1.59 percent) is also present on the Pacific side near the Bering Strait, while three New hot spots emerge at the edge of the cluster with two other outlying New hot spots are in northeastern Canada. Three large clusters are classified as Sporadic (22.76 percent), which fluctuates between hot and "neither hot nor cold" over time; one of these is on the Pacific side along with the main cluster, another is over eastern Greenland, and the third is over eastern Canada. Two Diminishing hot spots and eight Historic hot spot bins are barely noticeable on the southerly fringe of the large cluster over the Atlantic side of the Arctic basin.

Figure 5 also shows the centroid cold spots over this study area. These include the Sporadic (39.64 percent of the significant bins), New (<0.01 percent), Consecutive (<0.01 percent), and Oscillating (<0.01 percent) cold spots. Note that a New cold spot and a Consecutive cold spot are found over extreme southeastern Siberia. The EHSA shows how the location and intensity of the centroid clusters change over the Pacific and the Atlantic for the 1979─2017 period. These cluster positions also support the finding from the linear regression that the centroid position became increasingly static while drifting toward the Pacific.

Figure 6 shows the 1979─2017 change in intensity of hot and cold spots, by bin, according to the Mann-Kendall trend test. A total of 370 bins (of 3681, or 10.05 percent) show a significant uptrend, with 78, 160, and 132 of these significant respectively at the 99, 95, and 90 percent level. On the contrary, 498 bins (of 3681, or 13.53 percent) show significant downtrends, with 121, 200, and 177 of these significant respectively at the 99, 95, and 90 percent level.

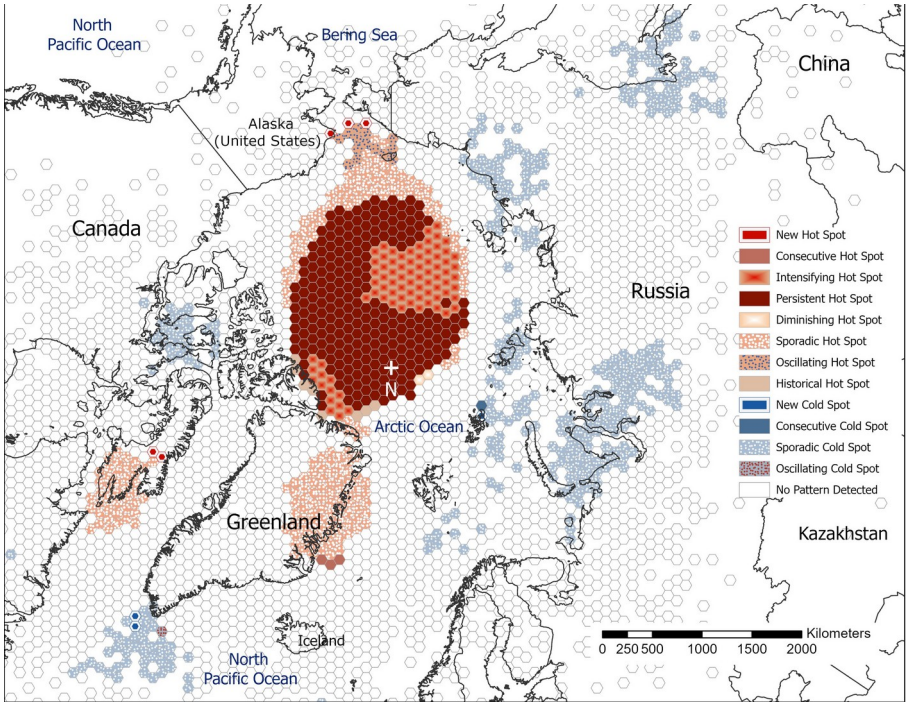

Figure 5. Categorization of NHCPV centroid position by hexagonal bin, based on significance of linear temporal trends, using emerging hot spot analysis, 1979–2017.

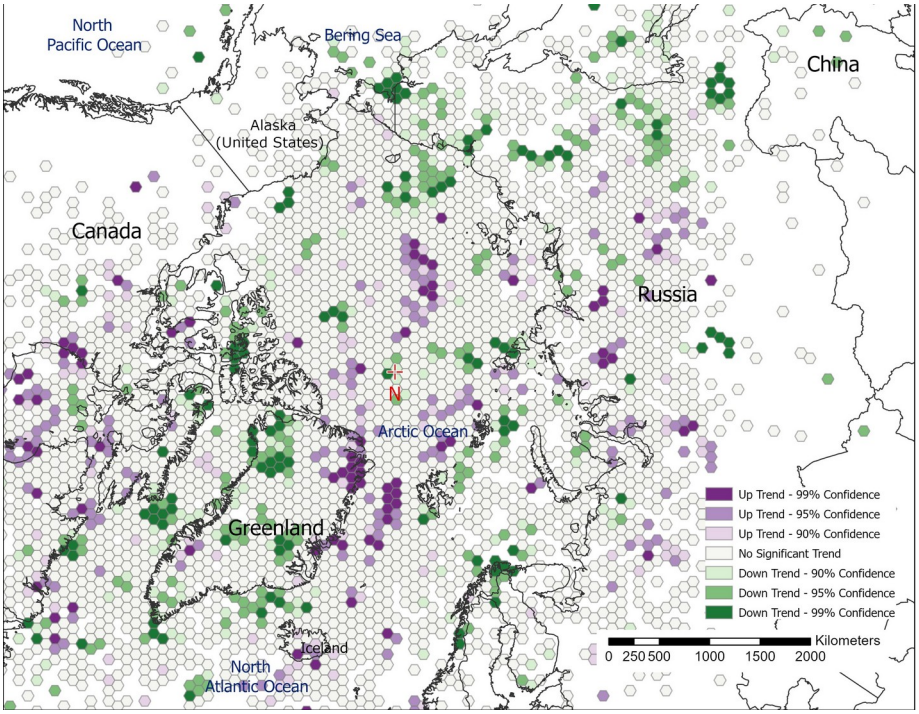

Figure 6. Linear temporal trends in the NHCPV centroid hot spot location intensities by bin, according to the Mann-Kendall statistics, 1979–2017.

352 To validate at the daily scale the findings of Wrona and Rohli (2007), who suggested that,
353 except in spring, the monthly mean centroid positions (1959─2001) tended to be displaced
354 toward the Pacific basin, the EHSA was performed over the 1979─2001 period and in segmented
355 intervals of 1979─1984, 1985─1990, 1991─1996, and 1997─2001. This analysis was also
356 conducted to validate the suggestion of Wrona and Rohli (2007) of low circular variability for
357 the centroid location, which implies that the centroid position moved little between 1959 and
358 2001.

359 Among the 1171 bins showing statistically significant (at a 95% confidence interval)
360 temporal trends over 1979─2001 period, nearly all were cold spots. The Oscillating cold spot
361 dominated these, with 601 bins, mostly over the Arctic basin with some elongation in the
362 Atlantic (Figure 7a). Of the remaining trending bins, 350 were Sporadic cold spots and 57 were
363 Consecutive cold spot (Figure 7a). Only 163 bins (16.17 percent) show no pattern over the
364 1979─2001 period, while 2798 (76.01 percent) display no pattern over the 1979─2017 period.
365 This vast difference may indicate that randomness in centroid positions increased as the daily
366 distance moved decreased. In the 2002─2017 interval (Figure 7b), the cold spots were virtually
367 absent, with Oscillating hot spot (368 bins) dominating the Arctic Basin. By contrast, the
368 Oscillating, Sporadic, and Consecutive cold spot bins decreased to 4, 5, and 0 bins, respectively.
369 The New hot spot emerged along with the core mostly on Pacific side with 10 bins and Sporadic
370 hot spot has only 1 bin (Figure 8a). Moreover, the emergence of New and other hot spots and
371 reduction of the cold spots indicates an overall trend toward hot spots.

372 Within the first half of the time series, the EHSA on segmented time periods (over
373 1979─1984, 1985─1990, 1991─1996, and 1997─2001; Figure 8a-d, respectively) suggests that
374 the number of Persistent hot spots decreased across the four segments while the Oscillating hot
375 spots increased suddenly in the 1997─2001 period. The number of New cold spots was high in
376 comparison to New hot spots, especially from 1979 to 1984, with the New cold spots skewed
377 toward the Arctic basin and north of Greenland (Figure 8a-d). On the contrary, the last four
378 segmented periods (2002─2005, 2006─2009, 2010─2013, and 2014─2017; Figure 9a-d,
379 respectively) show that the number of Sporadic and (to a lesser extent) Consecutive hot spots
380 increased abruptly in 2014─2017 (Figure 9d), and all these patterns are situated over the Pacific
381 basin side of the North Pole (Figure 9a-d). The time series of bin frequencies by segmented time
382 periods is shown in Figure 10.
383

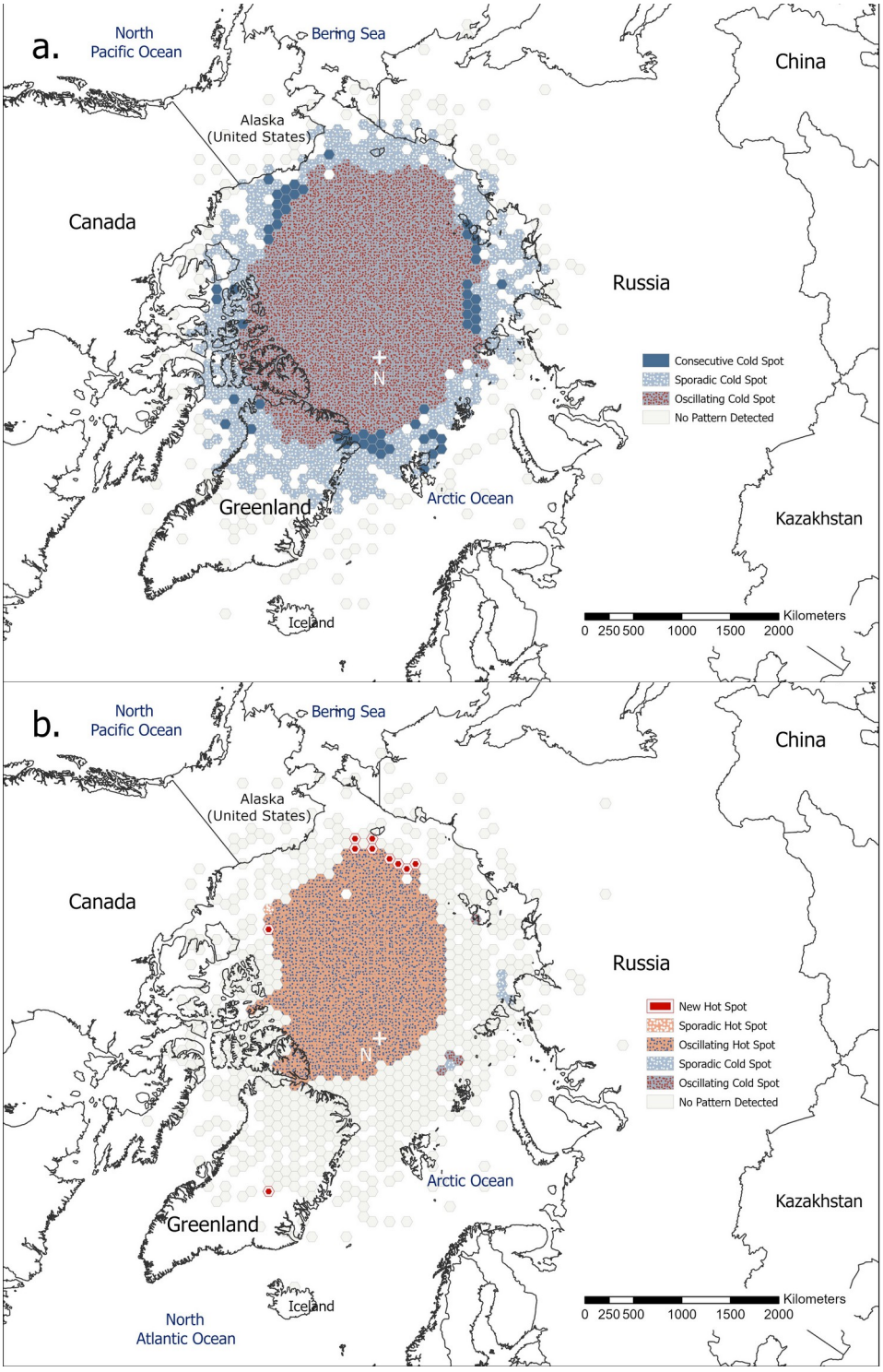

Figure 7. Emerging hot spot patterns showing the significant trends of centroid positions over (a) 1979–2001 and (b) 2002–2017.

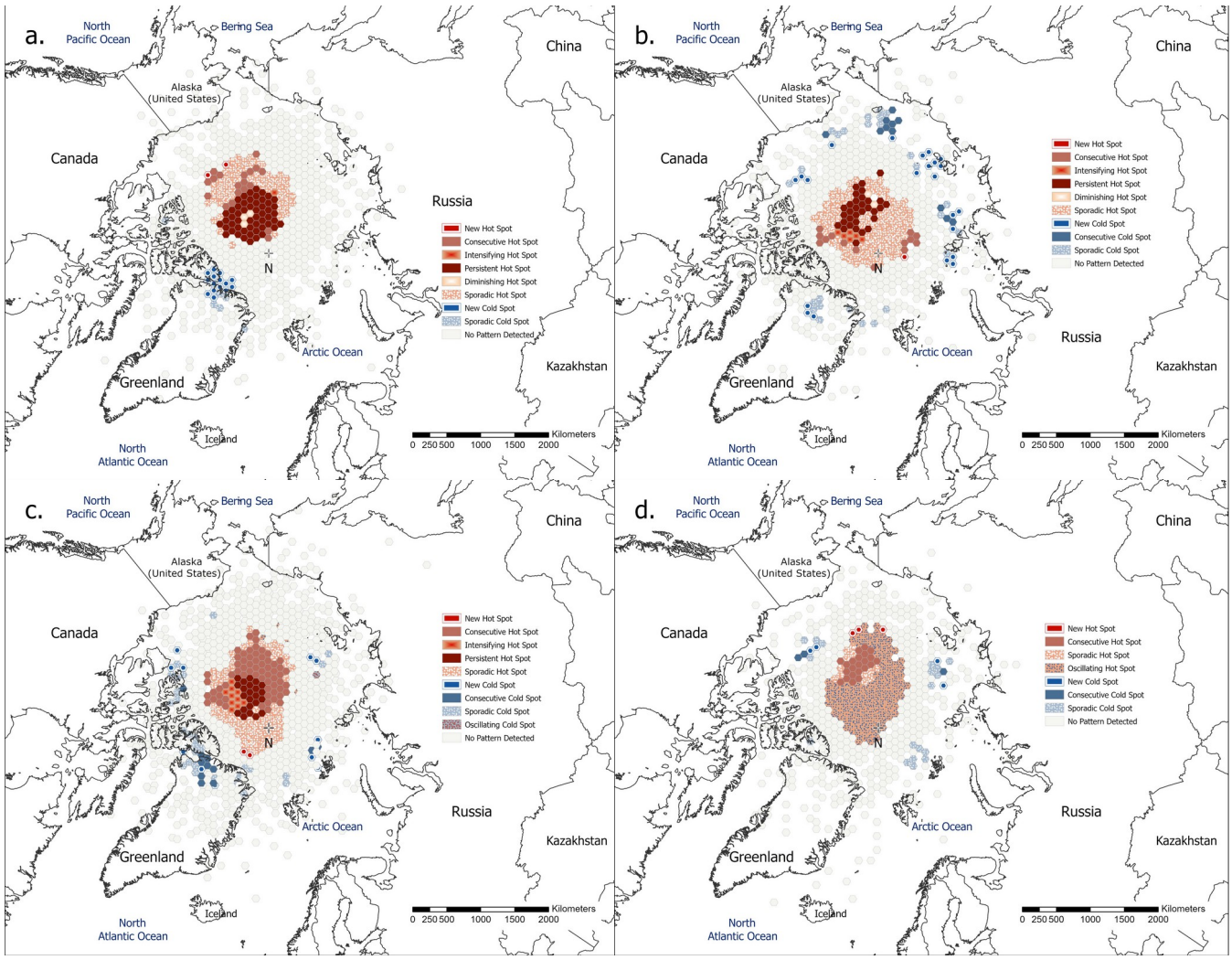

Figure 8. As in Figure 7, but for (a) 1979–1984, (b) 1985–1990, (c) 1991–1996, and (d) 1997–2001.

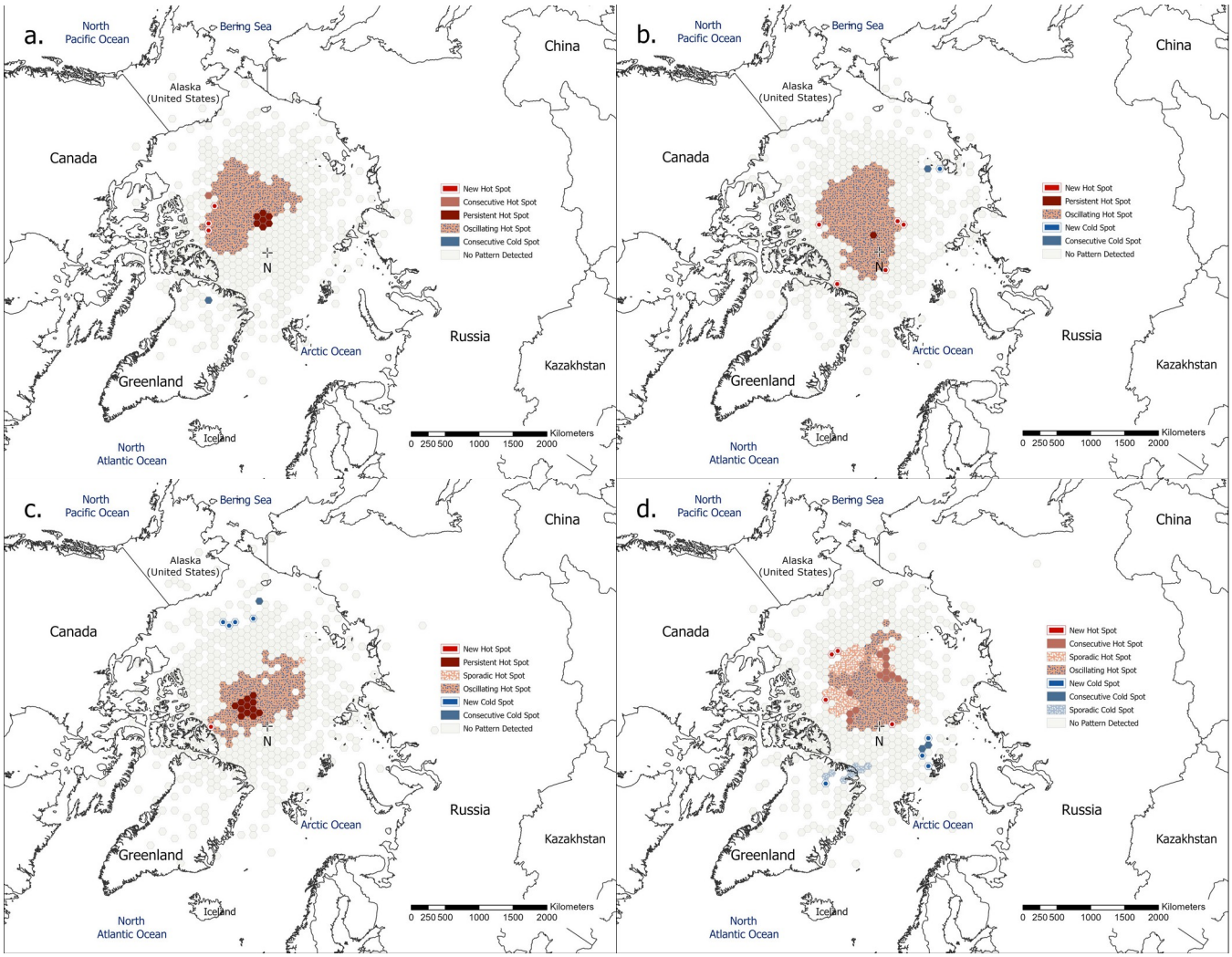

Figure 9. As in Figure 7, but for (a) 2002–2005, (b) 2006–2009, (c) 2010–2013, and (d) 2014–2017.

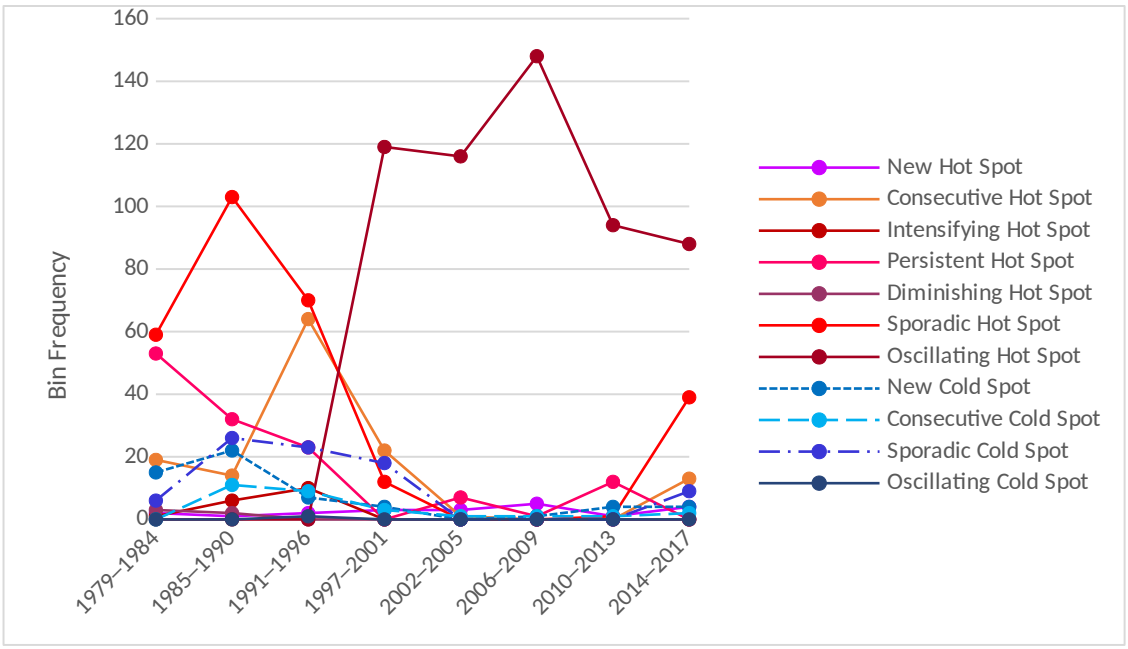

Figure 10. Number of bins by hot and cold spot categories for the NHCPV centroid location, by time period.

5 Summary and Conclusions

Studying the spatiotemporal CPV centroid characteristics is important for enhancing understanding in applications such as medium-to-long range weather forecasting, short-range climate prediction, and assessing impacts of atmosphere-ocean teleconnections such as the AMO and NAO. Linear trend analysis suggests that the day-to-day distance moved by the NHCPV centroid decreased significantly over time from 1979 to 2017, while there are persistent semi-annual and quarterly cycles visible throughout the time series but with different magnitudes. While the decreasing trend indicates stability in the positions of the centroid, the periodic cycle may provide an indication of the causes of perturbations such as weather pattern variability and extremes.

Over 1979─2017 period, EHSA identifies locations that are more likely (hot spots) and less likely (cold spots) for the NHCPV centroid, and temporal changes in the preference of such locations. A strong preference for hot spots toward the Pacific basin is notable across the study period. A number of hot and cold spots emerge and weaken over the last four decades, especially in the 1979─2001 sub-interval. Over the 2002─2017 period, the emerging hot spots were sufficient in number to skew the trend toward, according to the Mann-Kendall trend analysis over the 1979─2017 period.

Understanding spatio-temporal changes in centroid locations is useful, as Chen *et al.* (2015) noted the importance of such finite-amplitude wave activity for assessing future impacts of regional climate change. Future research will proceed with identifying the variability of the CPVs centroid positions at multiple atmospheric levels to consider the baroclinicity of the steering atmospheric circulation's response to continued surface warming, in the form of the NHCPV.

Acknowledgments, Samples, and Data

The authors are grateful for funding from Louisiana State University's Economic Development Assistantship and Dissertation Year Fellowship programs. Methods associated with the generation of the data used in this research, which characterize the NHCPV properties (i.e., CPV centroid location, area, and circularity, are described in more detail in Bushra and Rohli (2019), from the gridded data set obtained from the National Centers for Environmental Prediction (NCEP)/Department of Energy (DOE) Reanalysis 2 project. The data are available at https://www.esrl.noaa.gov/psd/data/gridded/data.ncep.reanalysis2.pressure.html.

References

Ayres, F. (1968). *Differential and Integral Calculus, Shaum's Outline Series*. McGraw-Hill Book Company, New York.

Bartlett, R. E., Bollasina, M. A., Booth, B. B., Dunstone, N. J., Marenco, F., Messori, G., & Bernie, D. J. (2018). Do differences in future sulfate emission pathways matter for near-term climate? A case study for the Asian monsoon. *Climate Dynamics*, *50*(5–6), 1863–1880. doi:10.1007/s00382-017-3726-6

Bushra, N., & Rohli, R. V. (2019). An objective procedure for delineating the circumpolar vortex. *Earth and Space Science*, *6*(5), 774–783. doi:10.1029/2019EA000590

Butterworth, S. (1930). On the theory of filter amplifiers. *Wireless Engineer*, *7*(6), 536–541.

Cassou, C., Terray, L., Hurrell, J. W., & Deser, C. (2004). North Atlantic winter climate regimes: Spatial asymmetry, stationarity with time, and oceanic forcing. *Journal of Climate*, *17*(5), 1055–1068. doi:10.1175/1520-0442(2004)017<1055:NAWCRS>2.0.CO;2

Chen, G., Lu, J., Burrows, D. A., & Leung, L. R. (2015). Local finite‐amplitude wave activity as an objective diagnostic of midlatitude extreme weather. *Geophysical Research Letters*, *42*(24), 10–952. doi:10.1002/2015GL066959

Chen, G., Peng, L., & Ma, C. (2018). Climatology and seasonality of upper ocean salinity: A three-dimensional view from argo floats. *Climate Dynamics*, *50*(5–6), 2169–2182. doi:10.1007/s00382-017-3742-6

De Smith, M. J., Goodchild, M. F., & Longley, P. (2007). *Geospatial Analysis: A Comprehensive Guide to Principles, Techniques and Software Tools*. Troubador Publishing Ltd.

Deakin, R. E., Bird, S. C., & Grenfell, R. I. (2002). The centroid? Where would you like it to be be? *Cartography*, *31*(2), 153–167. doi:10.1080/00690805.2002.9714213

Donohoe, A., Marshall, J., Ferreira, D., & Mcgee, D. (2013). The relationship between ITCZ location and cross-equatorial atmospheric heat transport: From the seasonal cycle to the Last Glacial Maximum. *Journal of Climate*, *26*(11), 3597–3618. doi:10.1175/JCLI-D-12-00467.1

Esri. (2020). *How Emerging Hot Spot Analysis works-ArcGIS Pro | Documentation*. Available from: https://pro.arcgis.com/en/pro-app/tool-reference/space-time-pattern-mining/learnmoreemerging.htm (Accessed 23 November 2020)

Esteban, P., Jones, P. D., Martín‐Vide, J., & Mases, M. (2005). Atmospheric circulation patterns related to heavy snowfall days in Andorra, Pyrenees. *International Journal of Climatology*, *25*(3), 319–329. doi:10.1002/joc.1103

Frauenfeld, O. W., Davis, R. E., & Mann, M. E. (2005). A distinctly interdecadal signal of Pacific Ocean–atmosphere interaction. *Journal of Climate*, *18*(11), 1709–1718. doi:10.1175/JCLI3367.1

Frierson, D. M., & Hwang, Y. T. (2012). Extratropical influence on ITCZ shifts in slab ocean simulations of global warming. *Journal of Climate*, *25*(2), 720–733. doi:10.1175/JCLI-D-11-00116.1

546 Getis, A., & Ord, J. K. (1992). The analysis of spatial association by use of distance statistics.
547 *Geographical Analysis*, *24*(3), 189–206. doi: 10.1111/j.1538-4632.1992.tb00261.x
548
549 GISGeography. (2020). *10 Open Source Remote Sensing Software Packages*. [online] Available
550 at: https://gisgeography.com/open-source-remote-sensing-software-packages/ [Accessed 12
551 October 2020].
552
553 Glovin, G. M., Arbetter, T. E., & Lynch, A. H. (2016). Wavelet analysis of polar vortex
554 variability over the twentieth century. *Journal of Geophysical Research–Atmospheres*, *121*(2),
555 722–732. doi:10.1002/2014JD022971
556
557 Hamed, K. H., & Rao, A. R. (1998). A modified Mann-Kendall trend test for autocorrelated
558 data. *Journal of Hydrology*, *204*(1–4), 182–196. doi:10.1016/S0022-1694(97)00125-X
559
560 Haskett, J. D., Pachepsky, Y. A., & Acock, B. (2000). Effect of climate and atmospheric change
561 on soybean water stress: A study of Iowa. *Ecological Modelling*, *135*(2–3), 265–277.
562 doi:10.1016/S0304-3800(00)00369-0
563
564 Hoskins, B., & D. Karoly (1981), The steady linear response of a spherical atmosphere to
565 thermal and orographic forcing. *Journal of the Atmospheric Sciences*, *38*(6), 1179–1196.
566 doi:10.1175/1520-0469(1981)038<1179:tslroa>2.0.co;2
567
568 Kanamitsu, M., Ebisuzaki, W., Woollen, J., Yang, S. K., Hnilo, J. J., Fiorino, M., & Potter, G. L.
569 (2002). NCEP-DOE AMIP-II Reanalysis (R-2). *Bulletin of the American Meteorological Society*,
570 *83*(11), 1631─1643. doi:10.1175/BAMS-83-11-1631
571
572 Kerr, R. A. (2000). A North Atlantic climate pacemaker for the centuries. *Science*, *288*(5473),
573 1984─1985. doi:10.1126/science.288.5473.1984
574
575 Kidston, J., Scaife, A. A., Hardiman, S. C., Mitchell, D. M., Butchart, N., Baldwin, M. P., &
576 Gray, L. J. (2015). Stratospheric influence on tropospheric jet streams, storm tracks and surface
577 weather. *Nature Geoscience*, *8*(6), 433─440. doi:10.1038/ngeo2424
578
579 Koopmans, L. H. (1995). *The Spectral Analysis of Time Series*. Elsevier.
580
581 Lamb, P. J., & Peppler, R. A. (1987). North Atlantic Oscillation: Concept and an
582 application. *Bulletin of the American Meteorological Society*, *68*(10), 1218–1225.
583 doi:10.1175/1520-0477(1987)068<1218:NAOCAA>2.0.CO;2
584
585 Levine, N. (2002). CrimeStat II: A spatial statistics program for the analysis of crime incident
586 locations (version 2.0). *Ned Levine & Associates, and the National Institute of Justice*: Houston,
587 TX and Washington, DC.
588
589 Liu, Q., Yan, C. R., Mei, X. R., Zhang, Y. Q., Yang, J. Y., & Liang, Y. S. (2012). Spatial
590 evolution of reference crop evapotranspiration in arid area of Northwest China. *Chinese Journal*
591 *of Agrometeorology*, *33*(1), 48–53.

Martin, J. E. (2015). Contraction of the Northern Hemisphere, lower-tropospheric, wintertime cold pool over the past 66 years. *Journal of Climate*, *28*(9), 3764–3778. doi:10.1175/JCLI-D-14-00496.1

Moron, V., Oueslati, B., Pohl, B., & Janicot, S. (2018). Daily weather types in February–June (1979–2016) and temperature variations in tropical North Africa. *Journal of Applied Meteorology and Climatology*, *57*(5), 1171–1195. doi:10.1175/JAMC-D-17-0105.1

Orme, L. C., Charman, D. J., Reinhardt, L., Jones, R. T., Mitchell, F. J., Stefanini, B. S., ... & Grosvenor, M. (2017). Past changes in the North Atlantic storm track driven by insolation and sea-ice forcing. *Geology*, *45*(4), 335–338. doi:10.1130/G38521.1

Rao, J. S. (1972). Some variants of chi-square for testing uniformity on the circle. *Zeitschrift für Wahrscheinlichkeitstheorie und verwandte Gebiete*, *22*(1), 33–44. doi:10.1007/BF00538904

Robusto, C. C. (1957). The cosine-haversine formula. *The American Mathematical Monthly*, *64*(1), 38–40. doi:10.2307/2309088

Rohli, R. V., Wrona, K. M., & McHugh, M. J. (2005). January northern hemisphere circumpolar vortex variability and its relationship with hemispheric temperature and regional teleconnections. *International Journal of Climatology*, *25*(11), 1421–1436. doi:10.1002/joc.1204

Sinnott, R. W. (1984). Virtues of the haversine. *Sky and Telescope*, *68*(2), 158.

Srinivas, G., Chowdary, J. S., Kosaka, Y., Gnanaseelan, C., Parekh, A., & Prasad, K. V. S. R. (2018). Influence of the Pacific–Japan pattern on Indian summer monsoon rainfall. *Journal of Climate*, *31*(10), 3943–3958. doi:10.1175/JCLI-D-17-0408.1

Steinbach, M., Tan, P. N., Kumar, V., Klooster, S., & Potter, C. (2003). Discovery of climate indices using clustering. In *Proceedings of the Ninth ACM SIGKDD International Conference on Knowledge Discovery and Data Mining*, pp. 446–455. doi:10.1145/956750.956801

Thompson, D. W., & Wallace, J. M. (1998). The Arctic Oscillation signature in the wintertime geopotential height and temperature fields. *Geophysical Research Letters*, *25*(9), 1297–1300. doi:10.1029/98GL00950

van den Broeke, M. R., & van Lipzig, N. P. M. (2002). Impact of polar vortex variability on the wintertime low-level climate of East Antarctica: Results of a regional climate model. *Tellus A: Dynamic Meteorology and Oceanography*, *54*(5), 485–496. doi: 10.3402/tellusa.v54i5.12161

Vanos, J. K., & Cakmak, S. (2014). Changing air mass frequencies in Canada: Potential links and implications for human health. *International Journal of Biometeorology*, *58*(2), 121–135. doi:10.1007/s00484-013-0634-2

638 Vincenty, T. (1975). Direct and inverse solutions of geodesics on the ellipsoid with application
639 of nested equations. *Survey Review*, *23*(176), 88–93. doi:10.1179/sre.1975.23.176.88
640
641 Wallace, J. M., & Gutzler, D. S. (1981). Teleconnections in the geopotential height field during
642 the Northern Hemisphere winter. *Monthly Weather Review*, *109*(4), 784–812. doi:10.1175/1520−
643 0493(1981)109<0784:TITGHF>2.0.CO;2
644
645 Wang, Z. Y., & Ding, Y. H. (2009). Impacts of the long-term change of the summer Asian polar
646 vortex on the circulation system and the water vapor transport in East Asia. *Chinese Journal of*
647 *Geophysics*, *52*(1), 20–29.
648
649 Waugh, D. W., Sobel, A. H., & Polvani, L. M. (2017). What is the polar vortex and how does it
650 influence weather? *Bulletin of the American Meteorological Society, 98*(1), 37–44. doi: 10.1175/
651 BAMS−D−15−00212.1
652
653 Welch, P. (1967). The use of fast Fourier transform for the estimation of power spectra: A
654 method based on time averaging over short, modified periodograms. *IEEE Transactions on*
655 *Audio and Electroacoustics*, *15*(2), 70–73. doi:10.1109/TAU.1967.1161901
656
657 Wrona, K. M., & Rohli, R. V. (2007). Seasonality of the northern hemisphere circumpolar
658 vortex. *International Journal of Climatology*, *27*(6), 697–713. doi:10.1002/joc.1430
659
660 Zhang, X., Ren, Y., Yin, Z. Y., Lin, Z., & Zheng, D. (2009). Spatial and temporal variation
661 patterns of reference evapotranspiration across the Qinghai−Tibetan Plateau during 1971–
662 2004. *Journal of Geophysical Research─Atmospheres*, *114*(D15). doi:10.1029/2009JD011753